Manipulating emission of CdSe/ZnS nanocrystals embedded in 3D photonic crystals

Céline Vion, Carlos Barthou, Paul Bénalloul, Catherine Schwob, Laurent Coolen, Alex Gruzintev, Gennadi Emelchenko, Wladimir Masalov, Jean-Marc Frigerio, Agnès Maître

Manipulating emission of CdSe/ZnS nanocrystals embedded in 3D photonic crystals

Céline Vion[1], Carlos Barthou[1], Paul Bénalloul[1], Catherine Schwob[1], Laurent Coolen[1], Alex Gruzintev[2], Gennadi Emelchenko[3], Wladimir Masalov[3], Jean-Marc Frigerio[1], and Agnès Maître[1]
(1) Institut des NanoSciences de Paris, UMR-CNRS 7588,
Université Pierre et Marie Curie, F-75015 Paris, France
(2) Institut of Microelectronics Technology and High Purity Materials,
Russian Academy of Science, 142432, Chernogolovka, Moscow District, Russia and
(3) Institute of Solid State Physics, Russian Academy of Science, 142432, Chernogolovka, Moscow District, Russia
(Dated: 2 juillet 2008)

We report experimental and theoretical results on the photoluminescence of CdSe/ZnS core-shell nanocrystals, embedded in a silica opaline structure by infiltration of a highly diluted solution. In comparison to the emission of nanocrystals in an homogeneous medium, strong modification of emission diagrams and increase of the lifetime (16%) of embedded nanocrystals have been observed. Those experimental results are compared to theoretical models, showing good agreement for the emission diagram. On the other hand, the lifetime variation cannot be explained just by modifications of photonic local density of states due to the photonic band gap, but modification of the dipole moment due to the local environment should be taken into account.

PACS numbers: 42.50.Nn ; 42.70.Qs, 61.72.uj ; 61.46.Hk ; 78.67.Bf

I. INTRODUCTION

Photonic crystals are characterized by a periodic dielectric constant at wavelength scale, creating photonic energy bands where light propagation is forbidden. The emission of light sources embedded inside a photonic crystal can be strongly affected by these bandgaps : according to Fermi's golden rule, the rate of spontaneous emission is proportional to the photonic local density of states (LDOS), which describes the interaction between emitters and the local field in the sample. As the photonic local density of states is strongly dependant on the material structure, photonic crystals are used for tailoring the emission of embedded light sources. This active field of research leads to applications ranging from quantum information processing [1], to light emitting devices (miniature lasers) [2] or solar cells [3].

Most devices use 2-dimensions (2D) photonic crystals, consisting in a lattice of holes etched in a high index transparent material. In the weak coupling regime, emission of single quantum dots in 2D photonic crystals has been improved, as well for their photoluminescence intensity [4] as for the polarization of emission [5]. In the strong coupling regime [6], achieved with InAs quantum dots embedded in a GaAs photonic crystal membrane, vacuum Rabi splitting [7] and emission of indistinguishable single photons [1] have been demonstrated. All these devices have been realized by electron lithography, requiring heavy technological equipments. Alternatively to this top-down approach, impregnation of 2D photonic crystals with solutions of colloïdal nanocrystals is a versatile way to couple emitters to photonic structures and to allow enhancement of spontaneous emission [8, 9].

Moreover, spontaneous self-organization of spherical colloidal particles is an attractive alternative to produce photonic crystals. Indeed, various techniques provide a low-cost and relatively easy protocol to obtain synthetic opals. It has been shown that the quality of opaline structures strongly depends on synthesis techniques [10]. Just as in 2D photonic crystals, the spontaneous emission of optical sources embedded in direct and inverted opals is affected by the crystal structure and can be inferred by the local density of states [11]. However, the modification of spontaneous emission lifetime by 3D silica opals is reported to be weak since the refractive index contrast is low (below 5% for an index contrast of 1.2) [12]. Larger effects require a higher refractive contrast and a complete photonic band gap which can be obtained in inverted opals [13–15]. For colloidal CdSe quantum dots infiltrated in titania inverse opals, lifetime reductions up to 30% have been reported [16]. Nevertheless, good quality inverse opals over large scale are still difficult to synthesize and most experimental studies on coupling emitters to 3D photonic crystals have been achieved in opals exhibiting a pseudo-band gap (infiltrated with quantum dots [17–22] or molecules [14, 23–25]).

Even incomplete, the photonic bandgap affects both the luminescence spectrum of the emitter and its spontaneous lifetime. Nevertheless, disorder in opal structures can hide or limit these phenomena. To get rid of the disorder, experiments have to be performed at a scale smaller than the typical size of the opal for which it can be considered a monocrystal. The use of a microscope can reveal the quality of the opals at a micronic scale by selection of a high quality opal zone [17, 25]. At this scale, stop-band effect on nanocrystals luminescence spectra [26], single nanocrystal emission modification [17] and sligth effects on luminescence lifetime [25] have been reported. Nevertheless the pseudo gap effect is averaged over the whole numerical aperture of the microscope objective, and the dip in fluorescence spectrum due to the gap disappears for a large aperture [23]. Therefore, the use of a microscope limits the possibilities

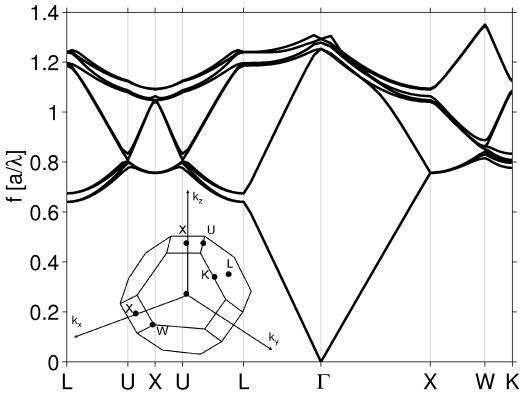

FIGURE 1: Photonic band structure of the fcc lattice calculated with effective index n_{eff}=1.34 as a function of reduced frequency $f = a/\lambda$ (where a is the primitive cell parameter $a = \sqrt{2}D$, with D the diameter of the balls), for wave vectors between the high symmetry points X, U, L, G, K and W of the Brillouin zone.

to study angle-resolved luminescent properties and does not reveal the quality of the opal over a large scale (mm) which is essential for applications.

The aim of this work is to study at macroscopic scale the coupling of colloidal core/shell CdSe/ZnS nanocrystals to artificial direct opals. In the first part, we present the preparation and optical characterization of opaline structures. The second section presents the modification of nanocrystals emission diagrams. In a third section, the influence of the stop band on the lifetime of CdSe/ZnS nanocrystal emission in the photonic crystal is analyzed experimentally and theoretically.

II. OPALS CHARACTERIZATION

The opals were prepared by sedimentation of 270 nm diameter silica balls in suspension in water, with a post selection of the 0.5 mm thick upper part of the deposit. The balls got organized spontaneously as a face-centered-cubic (fcc) structure according to the highest density plane (111). The samples were then dried at 150°C, and annealed at 600°C during 5 hours in free atmosphere. Robust 5x5x0.5 mm^3 samples were obtained ($\approx$ 2300 layers) [27, 28]. Fig. 1 presents the opal band diagram calculated numerically by a direct computation of the eigenstates and eigenvalues of Maxwell's equations (using a planewave basis) [29], showing a photonic pseudogap at the L point of the photonic Brillouin zone.

The opals were optically characterized by specular reflection, from which the diameter of the balls and the effective refracting index of the medium were inferred. The sample was illuminated with a fiberred and collimated halogen source covering the whole 350-800nm spectral range, and the reflected ligth was collected by a second optical fiber symmetric to the first one. The fibers were mounted on rotating stages allowing a precise selection of the incident and collection angles. The light spot on the opal had a size of $4mm^2$(at 20° incidence) and the distance between the sample and the optical fiber was 10 cm.

As the first bandgap of the direct opal is not complete, ligth propagation in this frequency range is allowed in certain directions and prohibited for others. Indeed, an important reflectivity is awaited for the wavelengths for which the phase difference induced by reflexions on two consecutive (111) planes of the face-centered cubic lattice is a multiple of 2π. This condition is fulfilled for an incidence angle corresponding to the Bragg angle which can be expressed as [30] :

$$\lambda_{max} = 2\sqrt{(2/3)}D\sqrt{(n_{eff}^2 - \sin^2(\phi))} \quad (1)$$

where D is the diameter of the balls, ϕ is the incidence angle relative to the normal of the (111) plane and n_{eff} is the effective refractive index of the medium with $n_{eff} = \sqrt{\alpha\epsilon_{silica} + (1-\alpha)\epsilon_0}$, and α is the filling factor ($\alpha = 0.74$ for close packed structures).

Fig. 2a presents the spectra obtained by specular reflexion on the opal for non polarized light at different incidence angles. The reflectivity is approximately 20% for frequencies inside the gap in spite of the large illuminated spot size which demonstrates a good quality of the samples over a large scale for the (111) planes. The wavelengths for which

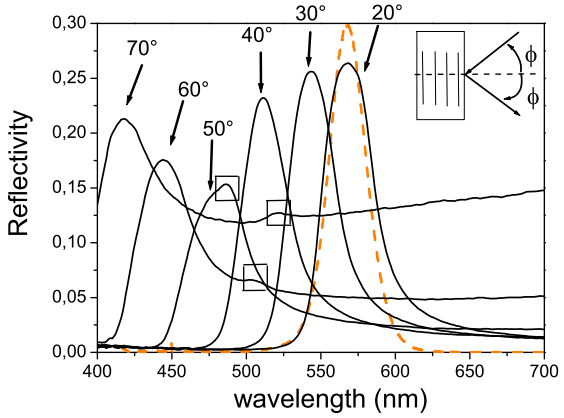

(a)

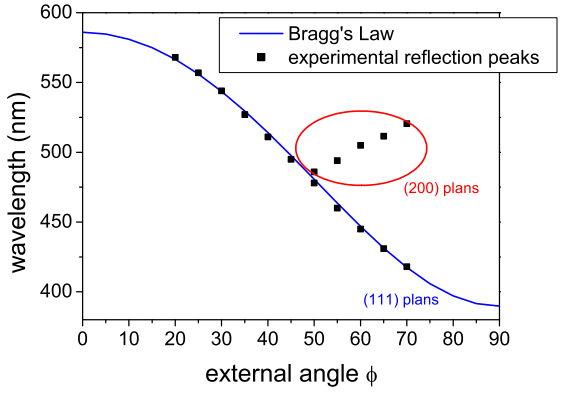

(b)

FIGURE 2: (a) Reflectivity spectrum of an opal for various incidence angles. (squares indicate the position of the second peaks) Dashed line : nanocrystals luminescence spectrum, (b) Comparison of the experimental results with Bragg's law 1 : D=269nm, n_{eff}=1.34

the specular reflectivity is maximum are plotted according to the angle of incidence. An adjustment with the Bragg's law (Fig. 2b) yields with a precision of 5%, the diameter of the balls $D = 269$ nm and the effective index of the structure $n_{eff} = 1.34$ corresponding to an index of the silica $n_{silica} = 1.44$. This diameter is in good agreement with the measurements performed with an atomic force microscope.

At an angle ϕ larger than 50°, a second peak appears on the reflection spectra (see Fig. 2.a). This peak unlike the first one shifts towards higher wavelengths for increased incident angles, as described in PMMA-sphere opals [31]. The interpretation of this phenomenon requires exact band structure calculations. On Fig. 3 the photonic band structure calculated along the LU and UX lines inside the first Brillouin zone (for $n_{eff} = 1.34$) is superimposed on the experimental peaks of specular reflection spectra as a function of the external incidence angle ϕ, which is related by Snell's law $\sin(\phi) = n_{eff}\sin(\theta)$ to the internal angle θ with the L direction normal to the (111) plane. At the U point (corresponding to an external angle ϕ of 50.2°), a second pseudo-gap can be attributed to the constructive interference reflections on the plane (200). The observation of this second peak, implying coherent reflections on other planes than the (111) ones, demonstrates the good face-cubic-centered crystallinity of the opal.

III. MODIFICATION OF NANOCRYSTALS EMISSION DIAGRAMS

We focus first on emission diagrams modification of nanocrystals embedded in the opal. We use a nanomolar solution of CdSe/ZnS nanocrystals (Qdot Invitrogen 565 ITK) diluted in decane of index $n_{decane} = 1.41$, a value close to the measured silica index ($n_{balls} = 1.44$). The luminescence spectrum of the solution is centered at 565 nm and presents a Full Width Half Maximum (FWHM) of 30 nm. The previously studied opal is infiltrated with $1\mu L$ of this solution and becomes translucent, demonstrating that the solution spread all over the opal : the decane infiltrated opal is

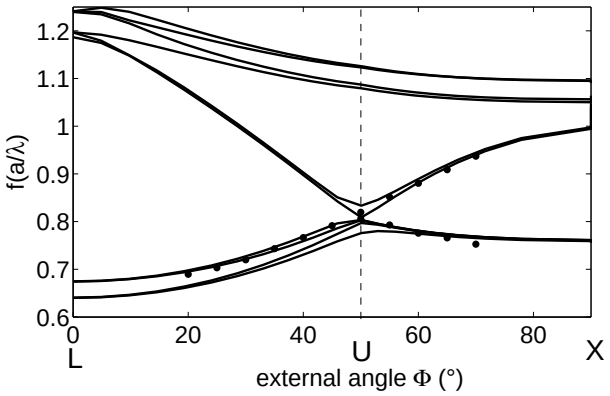

FIGURE 3: Photonic band structure (solid line) calculated along the LU and UX line expressed as a function of incidence angle. The circles indicate the experimental peaks associated with (111) and (200) planes.

close to an homogeneous medium with an effective index of 1.43. As a consequence, the nanocrystals are distributed randomly in the whole volume of the sample, with much less than one nanocrystal per void. Indeed, this low density of emitters prevents nanocrystals agregation and interactions among them, and the optical properties of the opal are not modified : after 15 min, the decane solution is totally evaporated, and specular reflection spectra realized on the infiltrated opal are identical to the ones realized prior to infiltration.

The infiltrated nanocrystals are then excited at a wavelength of 337.1 nm by a pulsed nitrogen laser (0.6 ns pulse width). Their luminescence is collected by an optical fiber mounted on a rotary stage and located at a distance of 10 cm from the surface. In this setup, for an illumination spot of $1mm^2$ size on the opal surface, the solid angle detection resolution is approximately 1°. The emission is analyzed with a spectrometer coupled to a nitrogen-cooled Si Charged-Coupled Device (CCD) detector. This setup has a wavelength resolution of 0.3 nm/point. The experimental specular spectra are plotted in Fig. 4a for different collection angles. As the FWHM of quantum dots luminescence spectrum is of the same order as the stop band FWMH, the incidence angle dependant gap does not induce a dip on luminescence spectra but induces a narrowing of the linewidth of the nanocrystal emission and a shift of the peak wavelength (see Fig. 4a). Depending of the angle of collection, the central wavelength of the emission line is shifted from 556nm to 566nm and the linewidth is reduced from 30 to 25 nm. In Fig. 4b, the radiation diagrams are plotted as a function of the angle of detection ϕ for different wavelengths. For each wavelength, a strong reduction of luminescence is observed for specific angles. In Fig. 5, these specific wavelengths for which quantum dots luminescence is reduced, are plotted as a function of the external angle ϕ. The curve is fitted by Bragg's law, like the central wavelength photonic bandgap measured previously by specular reflexion (Fig. 2). In order to confirm the influence of the crystalline structure, the opal is filled with a solution of decane, removing the gap. The dip in the emission diagram disappears for the decane filled sample, as expected for an homogeneous medium (Fig. 4c). These results are a clear demonstration of the modification of nanocrystals spontaneous emission diagrams by the photonic bandgap.

IV. MODIFICATION OF NANOCRYSTALS EMISSION LIFETIME

Let us now consider the influence of the photonic crystal on the nanocrystals decay rate. We experimentally compare the lifetime of nanocrystals embedded in an opal and in the same opal filled with a solution of decane which provides a uniform medium used as reference.

The experimental setup is the same as the one used for the luminescence study. The 560 nm emission line is selected by the spectrometer, and a photomultiplier provides lifetime measurement with a one nanosecond resolution. In the following, the fiber is settled orthogonal to the surface. Opals exhibit self-luminescence which is more than 100 times less intense than nanocrystals emission. Moreover, as seen on Fig. 6, the opal self luminescence decay is much faster than the quantum dot luminescence decay. For times shorter than 40 ns, the fast self-luminescence of silica balls influences the decay curves, and after 40 ns it become negligible. Therefore the nanocrystal luminescence lifetimes are calculated by fitting the decay curves for times between 40ns and 120ns.

The lifetime of the nanocrystals embedded in 269nm silica balls opal is $28ns \pm 1ns$. Then, the opal is infiltrated with decane in order to remove the photonic bandgap. The lifetime of the embedded nanocrystals becomes $24ns \pm 1ns$. The photonic bandgap is reversibly removed after evaporation of the decane, and the lifetime shifts again to 28 ns,

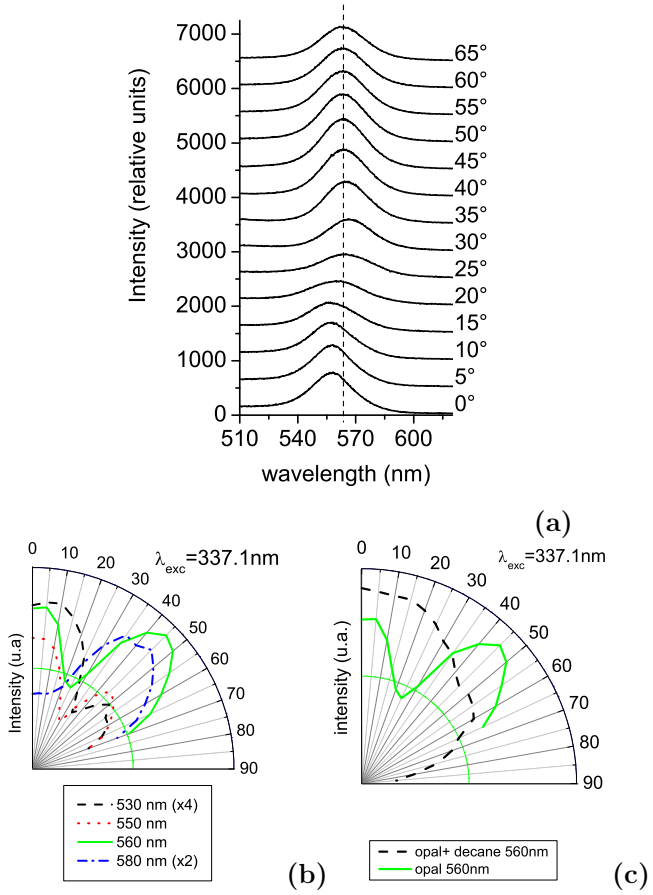

FIGURE 4: (a)Luminescence spectra of infiltrated nanocrystals in an opal sample at different collection angles (the spectra are shifted for clarity). (b)Diagrams of radiation of infiltrated nanocrystals at different wavelengths. (c)Diagrams of radiation at 560 nm of nanocrystals in opal (green plain line) compared to nanocrystals in opal infiltrated with decane (dashed black line).

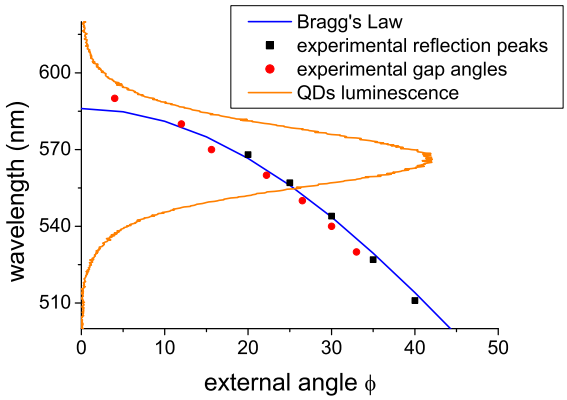

FIGURE 5: Comparison of the experimental results with Bragg's law. orange line : quantum dots in decane luminescence spectra. The red circles indicate the position of the minima on the diagrams of radiation. The black square are the position of the reflection maxima.

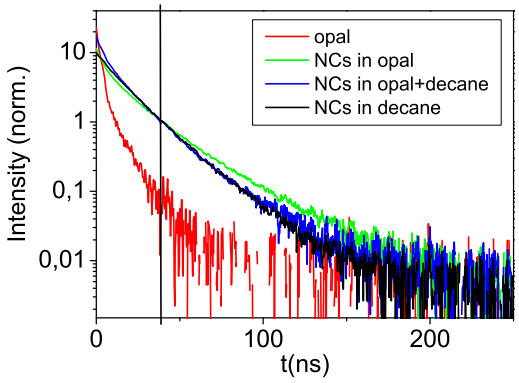

FIGURE 6: Luminescence decay of nanocrystals infiltrated in an opal (green line), dissolved in decane (black line), in the opal infiltrated with decane (blue line). Red line : self-luminescence of the opal.

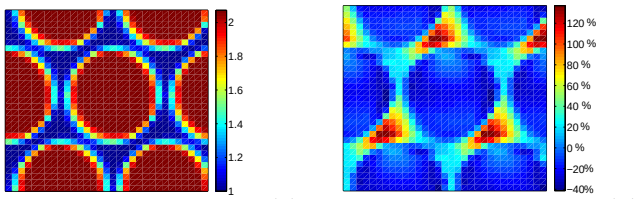

(a) (b)

FIGURE 7: (a) Assumed opal index on a plane (111). Calculation resolution : 17 nm. The transition zone between silica and air has a width of 51nm (b) Calculated percentage of variation of the local density of state around its mean value in the primitive cell at f=0.82.

demonstrating an experimental increase of the lifetime of 16%. In a second step, the same experiments are performed with similar nanocrystals , but this time, embedded in a 320 nm balls diameter opal, giving the same lifetime variation of 16%.

In order to explain these variations of lifetime, the variation of the local density of states at the emitters position has been calculated. According to Fermi's golden rule, the excited state of an emitting dipole decays exponentially to the ground state, with a decay constant :

$$\Gamma = 2\pi\rho(\omega, r, \vec{\mu}) = \frac{2\pi}{\hbar^2} \sum_{n,\vec{k}\in BZ} |\ \vec{\mu}\ .\ \vec{E_{\vec{k}}}\ (r)|^2 \delta(\omega - \omega_{n,\vec{k}}) \tag{2}$$

where $\vec{\mu}$ is the dipole moment, and $\vec{E_{\vec{k}(r)}}$, a plane wave function, is the electric field of mode $\vec{k}$. n refers to the number of the band. $\rho(\omega, \vec{r})$ is the photon LDOS and is strongly dependant on the environment. The dipole moment $\vec{\mu}$ is assumed to be randomly oriented in space.

Starting from the band diagrams, the distribution of electromagnetic field is calculated in the irreductible Brillouin zone by the standard plane-wave expansion method, and the LDOS inside the opal is inferred [12]. To improve the numerical accuracy, we used a linear interpolation technique as implemented within the abinit package [32] to obtain a stable numerical result with a small number of k points in the Brillouin zone. Then, we used 7106 k points in the first Brillouin zone (equivalent to 79507 equally spaced k points), the primitive cell being divided into 4096 segments, giving a resolution of 17 nm. For numerical reasons, the sharp transition between the silica index and the air index leads to diverging results and has to be replaced by a smoother one, of thickness equal to 3x17=51 nm (see Fig. 7a).

As seen on Fig. 7b, the LDOS variation $\rho(\omega, \vec{r})$ over the transition zone is 40% and can become larger than 100% between voids and inner silica balls. As a consequence, in the simulations, the exact localization of the nanocrystals, whose diameter(core+shell) is close to 10 nm, is critical. We assume that nanocrystals are randomly located in the three pixel interface between air and silica, and we calculate the average <LDOS>= $< \rho(\omega, \vec{r}) >$ over this intermediate region for which the index varies between 1.05 and the silica index 1.44.

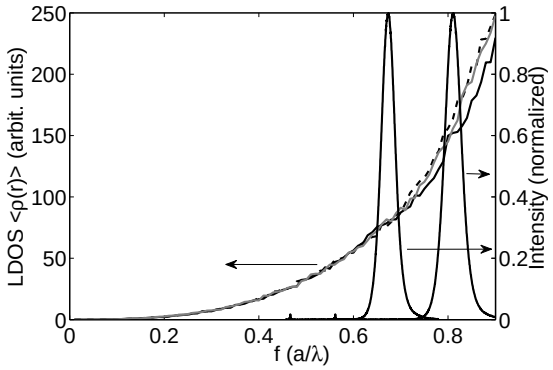

FIGURE 8: Averaged LDOS at air/SiO_2 interface for opal (full black line), opal filled with decane (dashed line), homogeneous medium of index n_{decane} (gray line). For the pure opal case , the LDOS is averaged on regions for which the index varies between 1.05 and 1.44. Luminescence spectra of nanocrystals emitting at 560nm as a function of the reduced frequency for 269nm ball size opal (left) and 320nm ball size opal (right).

On figure 8, the variation of <LDOS> with reduced frequency (a/λ) for an empty opal, an opal filled with decane and an homogeneous medium of index $n_{decane} = 1.41$ are compared. The <LDOS> for decane filled opal and homogenous medium are very close which is consistent with the previous observations on emission diagram(figure 4d). The <LDOS> scales as ω^3 as expected for an effective homogeneous medium. For an empty opal, two different regime have to be discussed. For a reduced frequency $f = a/\lambda < 0.62$, the averaged LDOS can be fitted by the $< LDOS >$ of an homogeneous medium of index 1.4 ± 0.05. In the band diagram of figure 1, $f = 0.62$ corresponds to the L point, for which the dispersion curve becomes different from the homogeneous medium, and the first photonic gap appears. For reduced frequencies larger than 0.62, the opal cannot be modelled by an homogenous medium and both the band diagram and the LDOS are modified by the crystalline structure of the opal. For f=0.82 the $< LDOS >$ exhibits a relative variation of 10% in comparison with the LDOS of the homogeneous medium of index 1.41. This difference increases from zero for f=0.62 to 15% for f=0.9. On Figure 8 the luminescence for 560 nm emitting nanocrystals is plotted as a function of the reduced frequency. For the 269 nm ball diameter opal the emission is centered at f=0.68, while for 320 nm ball diameter opal f=0.82.

Experimentally, for emission at f=0.82, the experimental increase of 16% of the embedded nanocrystal lifetime is in good agreement with the previous LDOS calculations. On the other hand, for f=0.68, where no lifetime modification is predicted, an experimental variation of 16% has also been observed. These results prove that this lifetime variation is due to an effect not fully taken into account in the LDOS calculation.

First, we emphasized the fact that the interface had to be replaced in the simulation by a smooth transition between silica balls and void, much larger than the size of the nanocrystals, and that the nanocrystals were randomly placed on this numerical transition zone. When the nanocrystal are supposed to be located inside this transition zone on the thinner region (17nm) of higher index, which in this case defines the interface, the predicted lifetime variation becomes as large as 20%, as it can be deduced from figure 7. Then, a more satisfactory simulation would consider a transition zone close to the size of the nanocrystal but would considerably increase the computation time.

Furthermore the infiltration of decane not only removes the index contrast but it can also change electronic interactions between nanocrystals and the material [12, 22]. The former calculations on LDOS suppose that the dipole moment $\vec{\mu}$ is randomly oriented and that its value is a constant whatever the environment is. However, it has been shown for single nanocrystals that their decay rates are strongly dependent on the local electronic environment [33]. Our lifetime measurement suggests that the variation of the dipole moment $\vec{\mu}$ may play a key role, which can hide the effect of the photonic band gap on the radiative lifetime.

V. CONCLUSIONS

Opals prepared by sedimentation techniques and infiltrated by colloidal semiconductors nanocrystals, have demonstrated a sufficient quality at a macroscopic scale, to induce a modification of the nanocrystal emission. Both the emission diagram and the lifetime are affected by the opal. Due to the crystalline structure, the variation of the

intensity with the collection angle is large and its dependance with the band structure has been modelled. Although lifetime modification has been simulated by a computation of the local density of states, experiments performed at different frequencies prove that its variation cannot be explained just by the opal photonic bandgap and that the electronic environment effect on the dipole moment $\vec{\mu}$ should not be neglected in the simulations.

A significant influence of the photonic bandgap on the lifetime would require a larger index contrast, or an inverse opal for which complete photonic bandgap can be achieved. The insertion of a defect [34, 35] inside opals, inducing a large modification of the LDOS, is a promising alternative to monitor the lifetime of nanocrystals embedded in 3D photonic crystals.

Acknowledgments

The authors gratefully acknowledge Karel Kunc for helpfull discussions and Emmanuelle Lacaze for AFM measurements. This study was supported by the Russian Foundation for Basic Research (projects N 07-02-90000 and N 07-02-92176) and C'Nano Ile de France.

[1] S. Laurent, S. Varoutsis, L. Le Gratiet, A. Lemaitre, I. Sagnes, F. Raineri, A. Levenson, I. Robert-Philip, and I. Abram, Applied Physics Letters 87 (2005).
[2] O. Gauthier-Lafaye, D. Mulin, S. Bonnefont, X. Checoury, J. Lourtioz, A. Talneau, and F. Lozes-Dupuy, IEEE Photonics Technology Letters 17, 1587 (2005).
[3] G. Ruani, C. Ancora, F. Corticelli, C. Dionigi, and C. Rossi, Solar Energy Materials and Solar Cells 92, 537 (2008).
[4] T. D. Happ, I. I. Tartakovskii, V. D. Kulakovskii, J.-P. Reithmaier, M. Kamp, and A. Forchel, Phys. Rev. B 66, 041303 (2002).
[5] W.-H. Chang, W.-Y. Chen, H.-S. Chang, T.-P. Hsieh, J.-I. Chyi, and T.-M. Hsu, Physical Review Letters 96, 117401 (2006).
[6] K. Hennessy, A. Badolato, M. Winger, D. Gerace, M. Atatuere, S. Gulde, S. Faelt, E. L. Hu, and A. Imamoglu, Nature 445, 896 (2007).
[7] T. Yoshie, A. Scherer, J. Hendrickson, G. Khitrova, H. Gibbs, G. Rupper, C. Ell, O. Shchekin, and D. Deppe, Nature 432, 200 (2004).
[8] N. Ganesh, W. Zhang, P. C. Mathias, E. Chow, J. A. N. T. Soares, V. Malyarchuk, A. D. Smith, and B. T. Cunningham, Nature Nanotechnology 2, 515 (2007).
[9] V. Reboud, N. Kehagias, M. Zelsmann, M. Striccoli, M. Tamborra, M. Curri, A. Agostiano, D. Mecerreyes, J. Alduncin, and C. Sotomayor Torres, Microelectronic Engineering 84, 1574 (2007).
[10] S. G. Romanov, M. Bardosova, D. E. Whitehead, I. M. Povey, M. Pemble, and C. M. S. Torres, Applied Physics Letters 90, 133101 (2007).
[11] E. Yablonovitch, Phys. Rev. Lett. 58, 2059 (1987).
[12] Z.-Y. Li and Z.-Q. Zhang, Phys. Rev. B 63, 125106 (2001).
[13] V. Solovyev, Journal of Applied Physics 94, 1205 (2003).
[14] M. Megens, J. E. G. J. Wijnhoven, A. Lagendijk, and W. L. Vos, Phys. Rev. A 59, 4727 (1999).
[15] I. S. Nikolaev, P. Lodahl, A. F. van Driel, A. F. Koenderink, and W. L. Vos, Phys. Rev. B 75, 115302 (2007).
[16] P. Lodahl, A. F. van Driel, I. S. Nikolaev, A. Irman, O. Karin, D. Vanmaekelbergh, and W. L. Vos, Letters to Nature 430, 654 (2004).
[17] M. Barth, R. Schuster, A. Gruber, and F. Cichos, Physical Review Letters 96, 243902 (2006).
[18] A. Blanco, C. Lopez, R. Mayoral, H. Miguez, F. Meseguer, A. Mifsud, and J. Herrero, Applied Physics Letters 73, 1781 (1998).
[19] Y. A. a. Valsov, Applied Physics Letters 71, 1616 (1997).
[20] Y. Lin, J. Zhang, E. H. Sargent, and E. Kumacheva, Applied Physics Letters 81, 3134 (2002).
[21] C. M. Chuang, W. B. Lu, W. F. Su, C. M. Lin, and Y. F. Chen, Journal of Applied Physics 97, 096104 (2005).
[22] K. Liu, T. Schmedake, K. Daneshvar, and R. Tsu, Microelectronics Journal 38, 700 (2007).
[23] S. Gaponenko, Journal of Luminescence 87-89, 152 (2000).
[24] S. G. Romanov, T. Maka, C. M. S. Torres, M. Müller, and R. Zentel, Journal of Applied Physics 91, 9426 (2002).
[25] R. A. L. Vallée, K. Baert, B. Kolaric, M. V. der Auweraer, and K. Clays, Phys. Rev. B 76, 045113 (2007).
[26] M. Barth, A. Gruber, and F. Cichos, Phys. Rev. B 72, 085129 (2005).
[27] M. Romanelli, C. Vion, C. Barthou, P. Benalloul, J. Frigerio, and A. Maitre, Journal of the Korean Physical Society 52, 1589 (2008).
[28] A. N. Gruzintsev, G. A. Emel'chenko, V. M. Masalov, M. Romanelli, C. Barthou, P. Benalloul, and A. Maitre, Inorganic Materials 44, 159 (2008).
[29] S. G. Johnson and J. D. Joannopoulos, Opt. Express 8, 173 (2001).
[30] Y. Xia, B. Gates, and S. Park, Journal of Lightwave Technology 17, 1956 (1999).

[31] S. G. Romanov, T. Maka, C. M. Sotomayor Torres, M. Müller, R. Zentel, D. Cassagne, J. Manzanares-Martinez, and C. Jouanin, Phys. Rev. E 63, 056603 (2001).
[32] X. Gonze, J. M. Beuken, R. Caracas, F. Detraux, M. Fuchs, G. M. Rignanese, L. Sindic, M. Verstraete, G. Zerah, F. Jollet, et al., Computational Materials Science 25, 478 (2002).
[33] L.-W. Wang, Journal of Physical Chemistry B 105, 2360 (2001), ISSN 1520-6106.
[34] P. Massée, S. Reculusa, K. Clays, and S. Ravaine, Chemical Physics Letters 422, 251 (2006).
[35] E. Palacios-Lidon, J. Galisteo-Lopez, B. Juarez, and C. Lopez, Advanced Materials 16, 341 (2004).